NASA-CR-202708

Computational Investigation of Tangential Slot Blowing on a Generic Chined Forebody

R. M. Agosta-Greenman, K. Gee,
R. M. Cummings, L. B. Schiff

Reprinted from

Journal of Aircraft

Volume 32, Number 4, Pages 811–817

A publication of the
American Institute of Aeronautics and Astronautics, Inc.
370 L'Enfant Promenade, SW
Washington, DC 20024-2518

JOURNAL OF AIRCRAFT
Vol. 32, No. 4, July–August 1995

Computational Investigation of Tangential Slot Blowing on a Generic Chined Forebody

Roxana M. Agosta-Greenman*
California Polytechnic State University, San Luis Obispo, California 93410
Ken Gee†
MCAT, Inc., Moffett Field, California 94035
Russell M. Cummings‡
California Polytechnic State University, San Luis Obispo, California 93407
and
Lewis B. Schiff§
NASA Ames Research Center, Moffett Field, California 94035

The effect of tangential slot blowing on the flowfield about a generic chined forebody at high angles of attack is investigated numerically using solutions of the thin-layer, Reynolds-averaged, Navier–Stokes equations. The effects of jet mass flow ratios, angle of attack, and blowing slot location in the axial and circumferential directions are studied. The computed results compare well with available wind-tunnel experimental data. Computational results show that for a given mass flow rate, the yawing moments generated by slot blowing increase as the body angle of attack increases. It is observed that greater changes in the yawing moments are produced by a slot located closest to the tip of the nose. Also, computational solutions show that inboard blowing across the top surface is more effective at generating yawing moments than blowing outboard from the bottom surface.

Nomenclature

C_n = yawing-moment coefficient, $n/q_\infty S_{ref} L_{ref}$
c_n = sectional yawing-moment coefficient
f_s = fuselage station, measured from the nose of body, Fig. 3
L_{ref} = reference length, body base width, $L_{ref} \equiv 8.086$ in., Fig. 3
MFR = jet mass flow ratio, $\rho_{jet} V_{jet} S_{jet} / \rho_\infty V_\infty S_{ref}$
M_{jet} = jet Mach number
M_∞ = freestream Mach number
n = yawing moment
q_∞ = freestream dynamic pressure, $q_\infty \equiv \frac{1}{2}\rho_\infty V_\infty^2$
Re_d = Reynolds number based on freestream conditions and body reference length, $\rho_\infty V_\infty L_{ref}/\mu_\infty$
S_{jet} = jet exit area, 0.005 in.^{2}
S_{ref} = reference area, body base area, 51.276 in.^{2}, Fig. 3
V_{jet} = jet velocity
V_∞ = freestream velocity
α = angle of attack
ΔC_n = incremental yawing-moment coefficient, $(C_n)_{blowing} - (C_n)_{no\ blowing}$
ξ, η, ζ = transformed coordinates in the axial, circumferential, and radial directions
μ_∞ = freestream coefficient of viscosity
ρ_{jet} = jet density
ρ_∞ = freestream density

Introduction

FUTURE aircraft designs will make use of the fixed separation points of a chined cross-sectional forebody, as utilized in the YF-22 and the YF-23 configurations. Wind-tunnel tests[1] show that the chined forebody produces more lift than the conventional forebody, even at poststall angles of attack. This is due to the additional planform area and the suction produced by the strong forebody vortices. These forebody vortices also give the chined forebody improved lateral-directional stability, which can be attributed to the upward shift of the leeward vortex.

As the flight envelope of present and future aircraft increases to include high-angle-of-attack flight, the need to understand the complex flowfield of an aircraft flying in this regime increases. The flowfield about a body at high angle of attack is dominated by large regions of three-dimensional separated flow. The boundary layer separates from the body and rolls up on the leeward side of the body to form strong vortices.[2] Possible vortex asymmetry in the flowfield can produce side force and yawing and rolling moments, which may lead to aircraft instability. As the aircraft angle of attack increases, the yaw control power required to coordinate a rolling maneuver increases to levels beyond those provided by conventional rudders (Fig. 1). Forebody flow control has the potential of providing additional directional control power at large angles of attack.

Forebody flow control can be obtained using mechanical or pneumatic methods. Experimental and numerical investigations show that both methods produce similar results.[1,3] One method currently being investigated is forebody tangential slot blowing.[4] In this method, air is blown tangential to

Presented as Paper 94-3475 at the AIAA Atmospheric Flight Mechanics Conference, Scottsdale, AZ, Aug. 1–2, 1994; received Sept. 1, 1994; revision received Feb. 2, 1995; accepted for publication Feb. 2, 1995.

*Graduate Research Assistant, Aeronautical Engineering Department; currently Research Scientist, NASA Ames Research Center, Applied Computational Aerodynamics Branch, Moffett Field, CA 94035. Member AIAA.
†Research Scientist. Member AIAA.
‡Department Chair and Professor. Associate Fellow AIAA.
§Special Assistant for High Alpha Technology. Associate Fellow AIAA.

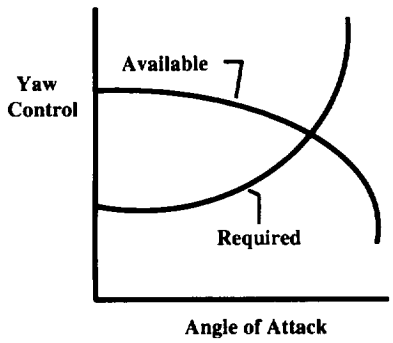

Fig. 1 Yaw control power.

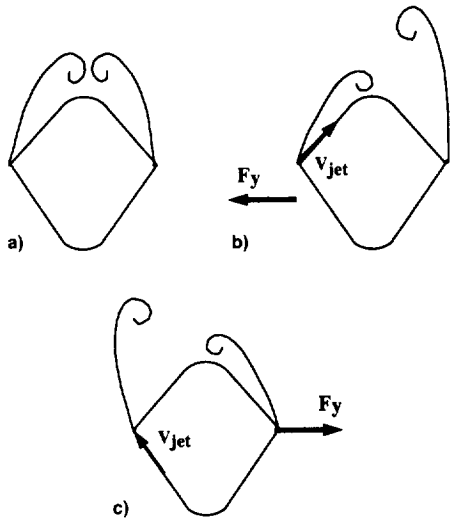

Fig. 2 Effects of tangential slot blowing on a chined forebody: a) no-blowing, b) blowing from the top surface, and c) blowing from the bottom surface.

the surface from a thin slot that is located on the forebody of the aircraft. Blowing inboard from a slot located on the top surface of the forebody disturbs the no-blowing flowfield (Fig. 2a) and draws the blowing-side vortex toward the surface, while the nonblowing-side vortex moves away from the surface (Fig. 2b). Blowing outboard from a slot located on the bottom surface (Fig. 2c) has a similar, but mirror effect. Here, the jet forces the blowing-side vortex away from the body surface, while the nonblowing-side vortex moves closer to the body. These changes in the flowfield generate side forces and yawing moments that have the potential of being employed to control the aircraft flying at high angles of attack.

A small-scale wind-tunnel experiment was recently performed[5] in the 3 ft × 4 ft Low Speed Wind Tunnel at California Polytechnic State University (Cal Poly) at San Luis Obispo to investigate the effectiveness of tangential slot blowing on a generic chined forebody. The dimensions of the wind tunnel model are shown in Fig. 3. The effects of varying slot lengths, jet mass flow ratios, and angles of attack were investigated. Experimental results obtained included measurement of total forces and moments as well as limited flow visualization.

In this study, a complementary computational fluid dynamics (CFD) investigation of tangential slot blowing is performed on the generic chined forebody model used in the Cal Poly wind-tunnel test. The effects of varying jet mass flow ratio, angle of attack, and blowing slot location (in both axial and circumferential directions) are studied. The numerical results are validated against the data obtained in the Cal Poly wind-tunnel experiment, and extend the study to slot configurations not tested in the wind tunnel.

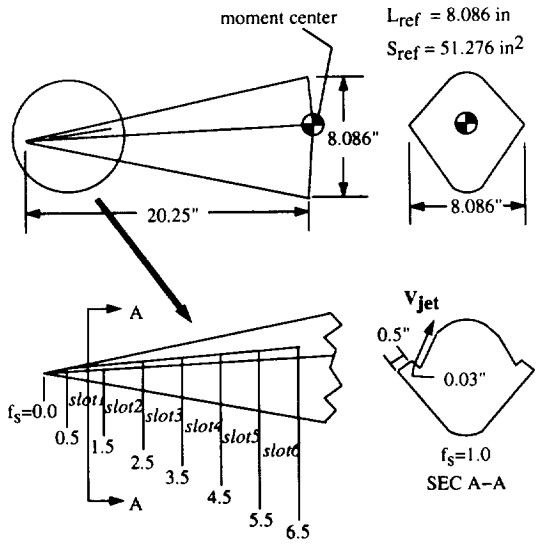

Fig. 3 Wind-tunnel model dimensions.

A brief discussion of the numerical method is presented in the next section, including the flow solver, computational grids, and boundary conditions. The results are then presented, from which conclusions are made about the effectiveness of tangential slot blowing as a means of forebody flow control.

Numerical Method

Governing Equations and Flow Solver

For flow about a body at high angle of attack with viscous effects and three-dimensional separated flow, the three-dimensional Navier–Stokes equations must be solved. In this study, the thin-layer, Reynolds-averaged Navier–Stokes equations are solved using the F3D code reported by Steger et al.[6] This code employs a two-factor, implicit, finite-difference algorithm utilizing an approximate-factored, partially flux-split scheme. The scheme uses upwind differencing in the streamwise direction ξ and central differencing in the circumferential η and radial ζ directions. The F3D code can have either first- or second-order accuracy in time, and has second-order accuracy in space. The F3D code has been used successfully to model the flow over bodies of revolution at high incidence and the flowfield over the F-18 aircraft.[4,7] Since the flow that is being studied is turbulent, the Baldwin–Lomax turbulence model,[8] with the modifications[9] that Degani and Schiff made to extend its applicability to high-alpha flows, is used. Additional details of the development of this code can be found in Refs. 6 and 10.

Computational Grids

Even with the large memory size available on modern supercomputers, it is not practical to use a single-zone body grid. Thus, the body grid is broken into four grids, two on each side of the body. In addition, two slot grids, one on each side of the body, are used to model the blowing slots. The Chimera overset grid scheme[11] is used to unite the body grids and slot grids. The body volume grid is shown in Fig. 4. The starboard and port sides of the body are symmetric. The two front body grids each consist of 40 axial points, 123 circumferential points, and 50 normal points; the two backbody grids each consist of 12 axial points, 123 circumferential points, and 50 normal points. The grid extends eight reference lengths normal to the body to minimize the effect of the inflow boundary on the flow near the body. The surface grid is clustered, as illustrated in Fig. 4, in regions where the flow gradients are expected to be the greatest. These regions include the chine area, where the flow is expected to separate.

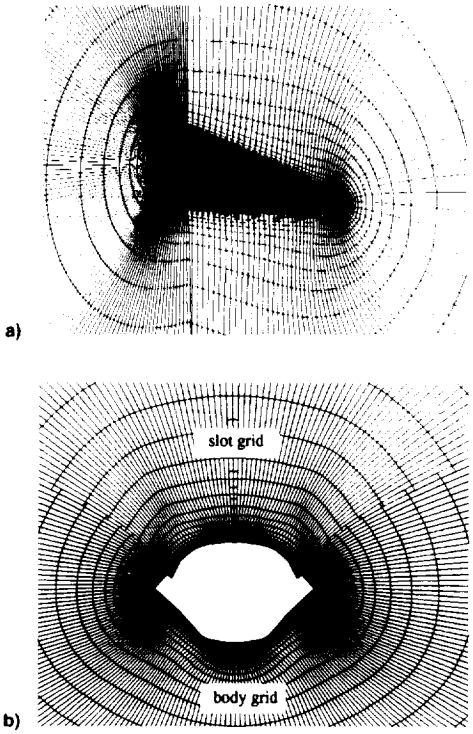

Fig. 4 Portion of grid modeling generic chined forebody and slots (every other point deleted for clarity): a) portion of computational grid and b) f_s = 10.

In the current study, two different multizone grid systems, each with four body and two slot zones, are created. One system models the slots located on the top surface of the body, which matches the experimental model, while the other grid system models the slots located on the bottom surface. For each slot configuration, identical slots are located on each side of the body. The grid modeling the slot on the top surface consists of 55 axial points, 40 circumferential points, and 39 normal points. The grid modeling the slot located on the bottom surface consists of 55 axial points, 86 circumferential points, and 39 normal points. The multizone computational grids for the top and bottom slot have a total of 811,200 and 1,008,540 points, respectively.

Boundary Conditions

On the body surface, which corresponds to the $\zeta = 1$ plane, no-slip and no-normal-velocity boundary conditions are enforced. Freestream conditions are maintained at the outer boundary of the grid. At the downstream outflow boundary, a simple zero-axial-gradient extrapolation condition is used.

Chimera[11] and Pegasus[12] are used to obtain boundary conditions at grid boundaries that overlap neighboring grids. In the outer boundaries of the slot grids, an overlap of approximately one grid point is used, except at the surface.

The jet in the slot grids is modeled computationally by using boundary conditions to introduce the jet exit conditions into the flowfield. If the jet exit Mach number is less than sonic, the jet total pressure and total temperature are input to the flow solver. The jet exit pressure is obtained by extrapolating the pressure from the local external flow at the jet exit. The jet exit Mach number is then obtained by using the isentropic relations for one-dimensional flow of an inviscid gas.[13] For sonic jets, the flow is assumed to choke at the exit and the jet pressure is obtained from isentropic relations using the jet total pressure and the total temperature. In either case, in order to match the experimental mass flow ratios, the total pressure of the jet is increased, thereby increasing the jet density, until the desired jet mass flow rate is obtained.

Initial Conditions

For no-blowing cases, the external flowfield is initially set to freestream values. The solution is advanced until a converged solution is obtained. The solution is considered converged when the L2 norms have dropped by two to three orders of magnitude. The blowing cases are started from the corresponding converged no-blowing solutions. This reduces the computational time necessary to converge the blowing solutions.

Results and Discussion

The F3D code is used to solve the flowfield about a generic chined forebody at two high angles of attack, α = 30 and 40 deg, at M_∞ = 0.2 and Re_d = 2.81 × 10^5. Comparisons are made with experimental data obtained at α = 30 and 40 deg, at M_∞ = 0.06 and Re_d = 2.81 × 10^5. The computational freestream Mach number is chosen to be higher than the experimental value to reduce computational convergence time. However, since both Mach numbers are low, compressibility effects are small,[13] and thus, the results can be compared. In all cases presented, the computed flow is treated as being fully turbulent.

No-Blowing Solutions

The major features of the computed no-blowing flowfield about the forebody at α = 40 deg are shown in Fig. 5. With no-blowing, the computed flowfield is symmetric. The surface flow pattern shows that primary crossflow separation lines occur at the chine line, and extend along the entire length of the body. In addition, the surface flow pattern shows that secondary and tertiary crossflow separation lines extend from the nose to the rear of the forebody. A fourth crossflow separation line appears near the rear of the forebody.

Figure 5 also shows computed helicity density contours in crossflow planes (normal to the axis of the forebody) at fuselage stations f_s = 1.0, 4.0, and 15.5. Helicity density is defined[14] as the scalar product of the local velocity and vorticity vectors, and is used to illustrate the size and shape of the vortices in the flowfield. The helicity density contours confirm that the flowfield is symmetric. The primary vortices originate from the primary crossflow separations at the chine line. The primary vortices grow larger and more diffuse with increasing axial distance. The primary vortices also move farther away from the forebody with increasing axial distance. The secondary vortices, which are smaller and weaker, lie

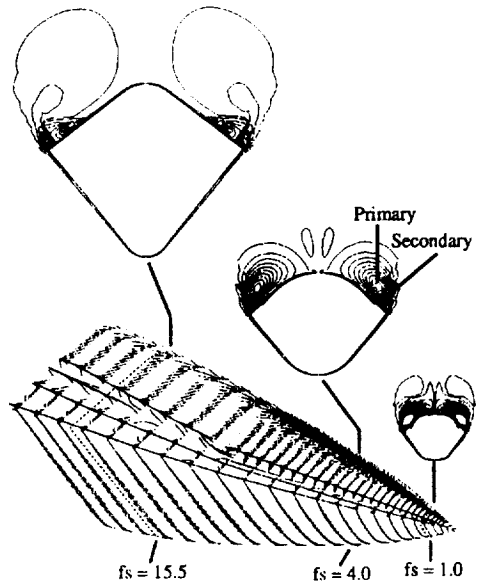

Fig. 5 Computed surface flow patterns and helicity density contours; no-blowing, M_∞ = 0.2, α = 40 deg, Re_d = 2.81 × 10^5.

underneath the primary vortices and rotate in the opposite direction to the primary vortices.

Blowing Solutions

Solutions were computed for flow about the forebody with tangential slot blowing from the starboard side (pilot's view) of the body. The blowing slot is 1 in. in length, starting 0.5 in. from the nosetip and extending aft. The slot is located on the upper surface of the chine (see Fig. 3) and the blowing was directed inboard toward the leeward symmetry plane, matching one of the slot configurations tested in the small-scale wind-tunnel[5] test. The computational jet MFRs were chosen to match those of the experiment.

Comparison of Numerical and Experimental Results

The computed forces and moments are obtained by integrating the surface-pressure distribution over the forebody. The moments are taken about a moment center located at the rear of the forebody (Fig. 3). To maintain consistency with the experiment,[5] incremental yawing-moment coefficients are presented next. Note that in all of the no-blowing computations, the resulting flowfield is symmetric and $(C_n)_{\text{no-blowing}}$ is zero. In the experiment, however, a small yawing moment was measured with zero blowing, probably due to slight model and tunnel installation asymmetries.

Figure 6 shows the effect on the incremental yawing moment as MFR increases at two angles of attack, α = 30 and 40 deg. As the angle of attack of the forebody is increased, the flowfield becomes more sensitive to perturbations. A greater change in the incremental yawing moment is produced for a given MFR as the angle of attack is increased. Both the present computations and the experiment[5] show this trend. Similar trends were observed in experiments using the F/A-18[15] and another chined forebody.[16] However, the experimental results for the current configuration did not show as great an increase in sensitivity as shown by the computed results.

For α = 30 deg, both the experimental and computational results (Fig. 6) show that the incremental yawing-moment coefficient increases smoothly as the jet mass flow ratio increases. The computational results underpredict the experimentally measured yawing moment. At α = 40 deg, however, the computed results show three distinct regions of effectiveness. In the first region (denoted as region I), low blowing rates produce a negative ΔC_n. In region II, this trend reverses, and ΔC_n increases with increasing MFR until a maximum is reached. In region III, further increases in MFR cause a reduction in ΔC_n. Similar trends have been observed in experiments using the F/A-18 with jet and slot blowing.[15] These regions will be discussed further in the following section. Note that for this angle of attack, the computed results are generally in better agreement with experiment than at α = 30 deg, except at the low MFR values.

Tangential slot blowing causes an asymmetric flowfield, resulting in an asymmetric surface-pressure distribution on the entire chined forebody, both on the upper (leeward) and lower (windward) sides. Examination of the pressure distributions on the forebody (not shown) indicates that the asymmetry on the upper surface is the major contributor to the resulting yawing moment. The contribution due to the upper surface is about twice that of the lower surface. Since the upper surface contributes the greatest asymmetry, and since our intent is to better understand the fluid dynamic phenomena causing the asymmetry, the following discussion concentrates on the interaction of the slot jet with the upper surface flowfield.

As stated, blowing becomes increasingly effective as the angle of attack is increased. This is apparent in the helicity density contours shown in Fig. 7. Helicity density contours in a crossflow plane at fuselage station f_s = 4.0 are shown for α = 30 and 40 deg. This crossflow plane is located just aft of the blowing slot. In the no-blowing solutions, the vortices are stronger at α = 40 deg (Fig. 7b) than at α = 30 deg (Fig. 7a). When blowing is turned on, the α = 30-deg case (Fig. 7c) shows that the primary vortex on the blowing side moves toward the surface, whereas the primary vortex on the non-blowing side moves away from the surface and becomes weaker as compared to the no-blowing solution (Fig. 7a). In the α = 40-deg case (Fig. 7d), movement of the primary vortex is similar to the α = 30-deg case, except that the changes in the strength of the vortices are larger. This bigger change, in turn, leads to larger values of ΔC_n. For tangential slot blowing it appears that both changes in strength and position of the vortices are important in the effectiveness of blowing. This is different from outward blowing where the change in vortex position is more effective than manipulating vortex strength.[17]

Analysis of Computational Flowfield

In order to understand the curious reversal of the yawing moment at low blowing rates, and the dropoff in yawing moment at the largest blowing rates, a blowing solution from each region shown in Fig. 6 is examined. These include the flows for MFR = 0.23×10^{-3} (region I), MFR = 1.49×10^{-3} (region II), and MFR = 4.17×10^{-3} (region III). The sectional yawing-moment coefficient distributions c_n along the body (Fig. 8) show the changes in the effect of blowing. At the lowest MFR (region I), c_n is negative for all stations along the body, and thus the total C_n is negative, as seen in Fig. 6.

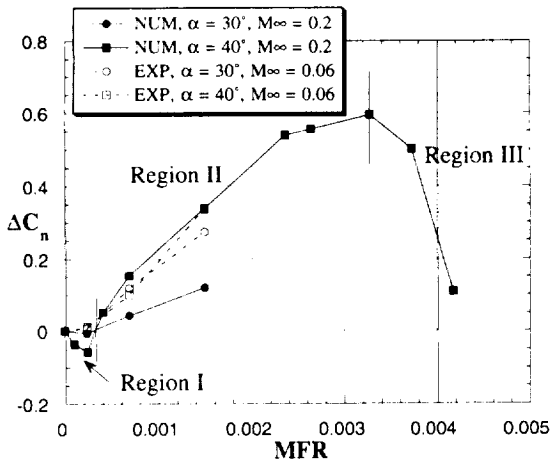

Fig. 6 Effect of angle of attack on yawing-moment coefficient produced by slot blowing; $Re_d = 2.81 \times 10^5$.

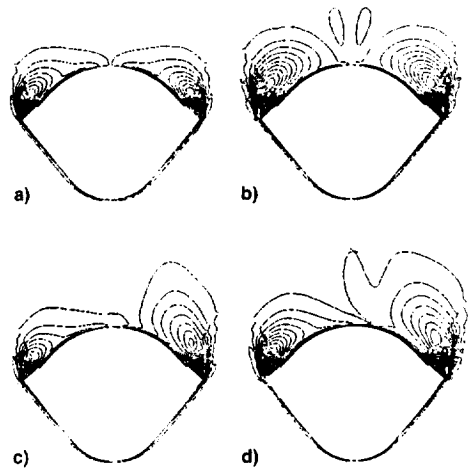

Fig. 7 Computed helicity density contours at fuselage station, f_s = 4.0; M_∞ = 0.2, $Re_d = 2.81 \times 10^5$: a) no-blowing, α = 30 deg; b) no-blowing, α = 40 deg; c) MFR = 1.49×10^{-3}, α = 30 deg; and d) MFR = 1.49×10^{-3}, α = 40 deg.

For MFR = 1.49 × 10^{-3} (region II), the sectional side force is always positive and increases with increasing axial distance, resulting in the yawing moment distribution shown in Fig. 8. For MFR = 4.17 × 10^{-3} (region III), the sectional yawing moment is negative in the blowing region and becomes positive downstream of the slot. However, the positive sectional c_n is much smaller than for MFR = 1.49 × 10^{-3}.

The behavior of the sectional yawing-moment distributions can be explained in part by examining the surface flow patterns and helicity density contours. The computed surface flow patterns near the nose (Fig. 9) show that at the lowest MFR (Fig. 9b) the secondary crossflow separation occurs inboard of the location observed in the no-blowing solution (Fig. 9a). The attachment lines appear to remain in approximately the same positions. In region II (Fig. 9c), the surface flow pattern shows that the jet remains attached to the blowing-side upper surface due to the Coanda effect. Also, the low momentum external flow is entrained by the jet. In the attached flow region, the surface pressure is lower than that at the corresponding points on the nonblowing side, which causes a side force toward the blowing side. Finally, in region III (Fig. 9d), the secondary separation line on the blowing side near the tip of the nose has been severely altered. There are no visible changes on the nonblowing side. The attachment lines move toward the nonblowing side of the forebody.

The corresponding helicity density contours, in a crossflow plane at f_s = 1.0 (in the slot region), are shown in Fig. 10. The no-blowing case (Fig. 10a) is symmetric, as described earlier. At MFR = 0.23 × 10^{-3} (Fig. 10b), the low-energy

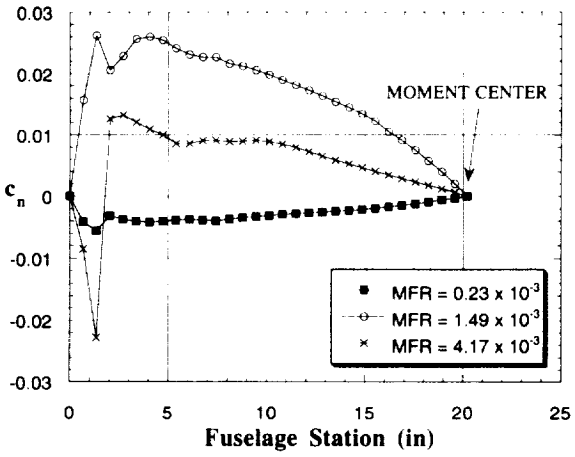

Fig. 8 Distribution of computed sectional yawing-moment coefficient along the body; M_∞ = 0.2, α = 40 deg, Re_d = 2.81 × 10^5.

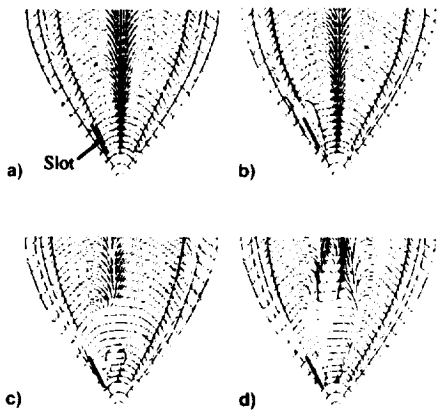

Fig. 9 Computed surface flow patterns; M_∞ = 0.2, α = 40 deg, Re_d = 2.81 × 10^5: a) no-blowing; b) region I, MFR = 0.23 × 10^{-3}; c) region II, MFR = 1.49 × 10^{-3}; and d) region III, MFR = 4.17 × 10^{-3}.

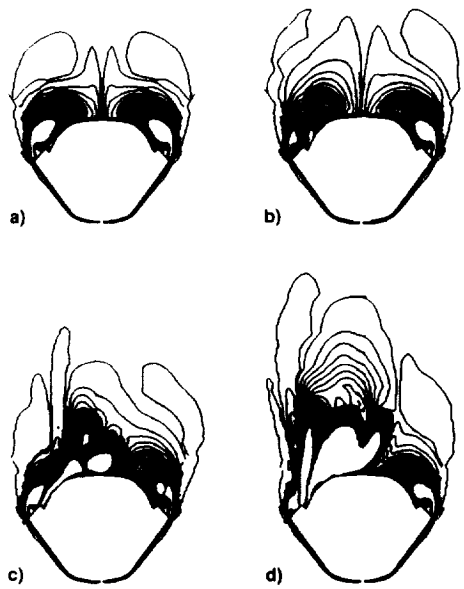

Fig. 10 Computed helicity density contours at f_s = 1.0; M_∞ = 0.2, α = 40 deg, Re_d = 2.81 × 10^5: a) no-blowing, b) region I, MFR = 2.32 × 10^{-4}; c) region II, MFR = 1.49 × 10^{-3}; d) region III, MFR = 4.17 × 10^{-3}.

jet causes the primary vortex on the blowing side to move away from the surface and the strength of the vortex is reduced. At the same time, the nonblowing-side vortex moves towards the surface, producing a small side force and yawing moment toward the nonblowing side of the body. For MFR = 1.49 × 10^{-3} (Fig. 10c), the primary vortex on the blowing side is entrained by the jet and moves downward towards the surface due to the Coanda effect. The nonblowing-side vortex moves away from the surface. Here, the movement of the vortices and the resulting lower pressure region on the blowing side cause a side force and yawing moment toward the blowing side. At the highest MFR, MFR = 4.17 × 10^{-3}, the jet is so strong that it acts to separate, rather than entrain, the blowing-side vortex flow (Fig. 10d). The blowing-side vortex moves away from the surface and the nonblowing-side vortex moves toward the surface. This causes c_n to be negative in the region of the jet, as shown in Fig. 8. At this high mass flow ratio, the pressure at the jet exit is about 10 times greater than the freestream pressure. Hence, the jet rapidly expands after leaving the blowing slot, which causes the jet to separate, and pushes the primary vortex away from the surface.

Effect of Axial Location of the Blowing Slot

It is recognized[1,5,18] that perturbations located close to the nose are more effective in developing asymmetric flows over the body than disturbances located further downstream. In the wind-tunnel experiment conducted at Cal Poly,[5] it was found that the most effective slot configuration of those tested on the generic chined forebody was a slot 1 in. long, located 0.5 in. from the tip of the nose (referred to as slot 1), and blowing tangentially toward the leeward symmetry plane. To investigate the effect of axial slot location computationally, solutions were obtained for an additional slot configuration (which had also been tested experimentally). This slot (referred to as slot 2) had the same 1 in. length as slot 1, but extended rearward from a point 1.5 in. from the tip of the nose (see Fig. 3).

The variation of ΔC_n with MFR (Fig. 11) for the two slot configurations is similar. The computed results for both slot configurations show a force reversal at low MFRs, followed by increasing ΔC_n with increasing MFR. Slot 1 produces a larger magnitude of ΔC_n for a given MFR than does slot 2. This trend is clearly seen at the higher MFRs, and was seen

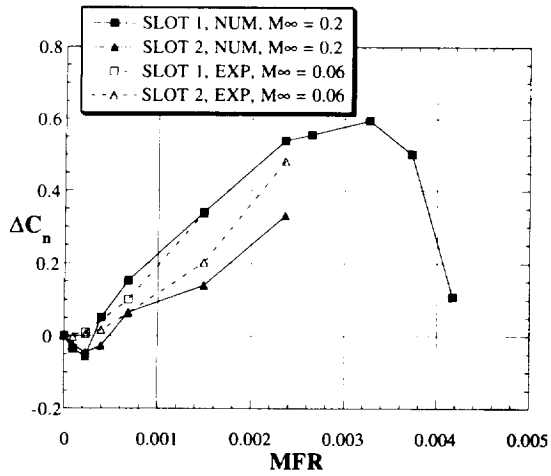

Fig. 11 Effect of axial slot location on yawing-moment coefficient, α = 40 deg, Re_d = 2.81 × 10^5.

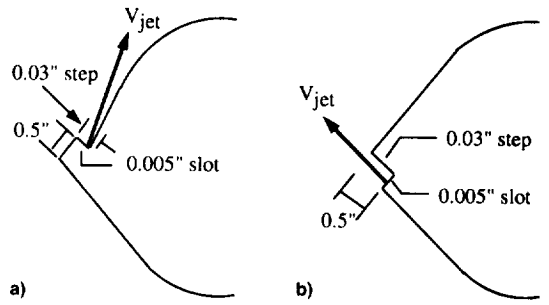

Fig. 12 Slot configurations for a) top- and b) bottom-slot blowing.

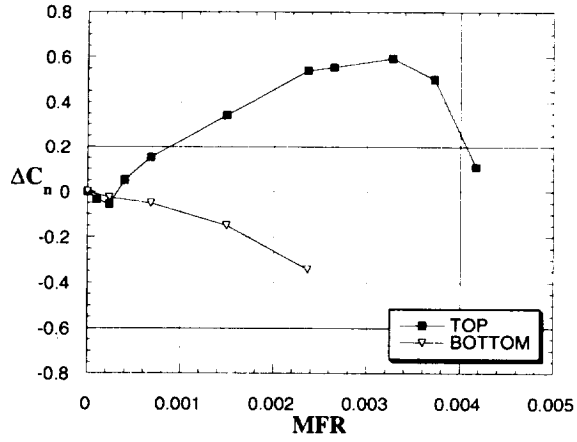

Fig. 13 Effect of circumferential slot location on yawing-moment coefficient; M_∞ = 0.2, α = 40 deg, Re_d = 2.81 × 10^5.

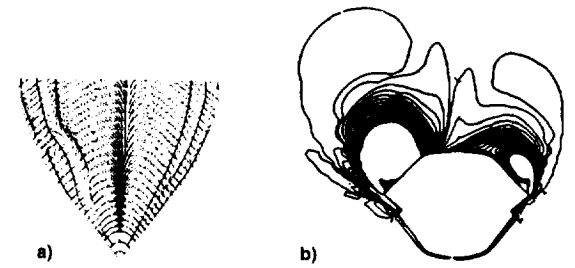

Fig. 14 Computed surface flow pattern and helicity density contours for bottom-slot blowing; M_∞ = 0.2, α = 40 deg, Re_d = 2.81 × 10^5, MFR = 1.49 × 10^{-3}: a) surface flow pattern and b) helicity density countours, f_s = 1.0.

in both the numerical and experimental results. It is also consistent with results obtained by Degani and Schiff,[18] who found that small disturbances near the tip of the nose produce greater effects on the flowfield than disturbances placed further aft.

Effect of Circumferential Location of the Blowing Slot

Only one circumferential slot location, on the upper chine surface and blowing inboard, was tested in the experiment of Ref. 5. In order to determine whether an alternative circumferential slot location could be more effective in developing side forces and yawing moments on the body, computations were carried out for a slot located on the lower chine surface and blowing tangentially outboard (Fig. 12). This slot had the same axial location and extent of slot 1. For the configurations investigated, it was found that blowing from the bottom slot produces a side force and yawing moment directed away from the blowing side (Fig. 2). Blowing from the upper slot produces a greater change in yawing-moment coefficient for a given MFR than does blowing from the bottom slot (Fig. 13). At the low MFRs blowing from the upper slot produces a force reversal; however, this is not found in the bottom-blowing results. This is probably due to the different method by which force is generated. Blowing from the bottom does not require entrainment of the vortex towards the surface whereas top blowing requires the vortex to move closer to the surface. Therefore with bottom blowing, at low MFR values, the blowing-side vortex is still pushed away from the surface.

Figure 14 presents the surface flow pattern and helicity density contours for bottom-slot blowing at MFR = 1.49 × 10^{-3}, analogous to those shown for upper-slot blowing in Figs. 9c and 10c, respectively. Comparing the surface flow patterns for blowing from the top (Fig. 9c) and bottom (Fig. 14a) slots show that, in the bottom-blowing case, the secondary and tertiary separation lines immediately aft of the blowing region are moved towards the leeward plane of symmetry. In both blowing cases, the separation line locations in the aft portion of the forebody do not differ substantially from the no-blowing results. The helicity density contours obtained for the bottom-blowing case (Fig. 14b) show that in contrast to the upper-slot blowing case (Fig. 10c), the blowing-side vortex moves away from the surface and the nonblowing-side vortex moves closer to the surface.

Conclusions

A computational investigation of tangential slot blowing for forebody flow control on a generic chined forebody has been performed. The effects of several parameters on the ability of pneumatic flow control to generate side forces and yawing moments on a forebody with fixed separation lines were studied. These parameters include jet mass flow ratios, angle of attack, and slot position in the axial and circumferential direction. The computed results were compared with available wind-tunnel test data to determine the accuracy of the numerical analysis.

The computational and experimental results indicate that at a given mass flow rate, the side forces and yawing moments generated by slot blowing increase as the body angle of attack increases. At high angles of attack, the flow becomes highly sensitive to small changes in the geometry or flowfield. Therefore, for a given perturbation, in this case the jet, a larger change was produced as the angle of attack increased.

The computations indicate that at α = 30 deg, the side forces and yawing moments generated by slot blowing were positive and increased as the jet mass flow ratio increased. At α = 40 deg, three distinct regions were observed in the computational results. At low MFRs tangential slot blowing produces a negative side force and nose-left yawing moment. This is caused by the inability of the low-energy jet to move the vortices on the blowing side toward the surface. In the

next region, the jet has enough energy to entrain the blowing-side vortex, and the side force and the yawing moments are positive and increase as MFR increases. At still higher MFRs, the jet is underexpanded and pushes the blowing-side vortex away from the body, causing a dropoff in the side force and yawing moment.

The computational and experimental results show that a greater change of side forces and yawing moments are produced by a slot located closer to the tip of the nose than for the same length slot located farther aft on the body. Also, computations carried out for two different circumferential slot locations showed that at a given mass flow ratio and angle of attack, tangential slot blowing from the top surface slot was more effective at generating yawing moments than was blowing from the bottom surface slot.

Acknowledgment

This research was partially funded by NASA Grant NCA2-626.

References

[1]Boalbey, R. E., Ely, W., and Hahne, D. E., "High Angle of Attack Stability and Control Concepts for Supercruise Fighters," *High-Angle-of-Attack Technology*, 1992, pp. 759–784, NASA CP-3149.

[2]Schiff, L. B., Cummings, R. M., Sorenson, R. L., and Rizk, Y. M., "Numerical Simulation of High-Incidence Flow over the Isolated F-18 Fuselage Forebody," *Journal of Aircraft*, Vol. 28, No. 10, 1991, pp. 609–617.

[3]Rao, D. M., and Puram, C. K., "Chine Forebody Vortex Manipulation by Mechanical and Pneumatic Techniques on a Delta Wing Configuration," AIAA Paper 91-1812, June 1991.

[4]Gee, K., Rizk, Y. M., Murman, S. M., Lanser, W. R., Meyn, L. A., and Schiff, L. B., "Analysis of a Pneumatic Forebody Flow Control Concept About a Full Aircraft Geometry," AIAA Paper 92-2678, June 1992.

[5]Cummings, R. M., Schiff, L. B., and Duino, J., "Experimental Investigation of Tangential Slot Blowing on a Generic Chined Forebody," AIAA Paper 94-3477, Aug. 1994.

[6]Steger, J. L., Ying, S. X., and Schiff, L. B., "A Partially Flux Split Algorithm for Numerical Simulation of Compressible Inviscid and Viscous Flow," *Proceedings of the Workshop on Numerical Methods in Fluid Dynamics*, Davis, CA, June 1986.

[7]Murman, S. M., Schiff, L. B., and Rizk, Y. M., "Numerical Simulation of the Flow About an F-18 Aircraft in the High-Alpha Regime," AIAA Paper 93-3405, Aug. 1993.

[8]Baldwin, B., and Lomax, H., "Thin-Layer Approximation and Algebraic Model for Separated Turbulent Flows," AIAA Paper 78-257, Jan. 1978.

[9]Degani, D., and Schiff, L. B., "Computation of Turbulent Supersonic Flows Around Pointed Bodies Having Crossflow Separation," *Journal of Computational Physics*, Vol. 66, No. 1, 1986, pp. 173–196.

[10]Ying, S. X., "Three-Dimensional Implicit Approximately Factored Schemes for Equations in Gasdynamics," Ph.D. Dissertation, Stanford Univ., Stanford, CA, 1986; also SUDAAR 557, June 1986.

[11]Benek, J. A., Buning, P. G., and Steger, J. L., "A 3-D Chimera Grid Embedding Technique," AIAA Paper 85-1523, July 1985.

[12]Benek, J. A., Steger, J. L., Dougherty, F. C., and Buning, P. G., "Chimera: A Grid Embedding Technique," Arnold Engineering Development Center, AEDC-TR-85-64, Arnold Air Force Station, TN, 1986.

[13]Anderson, J. D., *Fundamentals of Aerodynamics*, McGraw-Hill, New York, 1991.

[14]Levy, Y., Degani, D., and Seginer, A., "Graphical Visualization of Vortical Flows by Means of Helicity," *AIAA Journal*, Vol. 28, No. 8, 1990, pp. 1347–1352.

[15]Kramer, B. R., Suárez, C. J., Malcolm, G. N., and James, K. D., "Forebody Vortex Control with Jet and Slot Blowing on an F/A-18," AIAA Paper 93-3449, Aug. 1993.

[16]Wurtzler, K., "Numerical Analysis of a Chined Forebody with Asymmetric Slot Blowing," AIAA Paper 94-0171, Jan. 1994.

[17]Boalbey, R. E., Ely, W. L., and Robinson, B. A., "A Sensitivity Study for Pneumatic Vortex Control on a Chined Forebody," AIAA Paper 93-0049, Jan. 1993.

[18]Degani, D., and Schiff, L. B., "Numerical Simulation of the Effect of Spatial Disturbances on Vortex Asymmetry," *AIAA Journal*, Vol. 29, No. 3, 1991, pp. 344–352.